INORGANIC CHEMISTRY FRONTIERS

RESEARCH ARTICLE

View Article Online
View Journal | View Issue

Cite this: *Inorg. Chem. Front.*, 2023, **10**, 1552

Sacrificial ligand route to hybrid polythiophene–silver nanoparticles for sinter-free conductive inks†

Juraj Drzic, [a] Alberto Escudero, *[a,b] Lola González-García [a,c] and Tobias Kraus *[a,d]

We report the synthesis of AgNP@PEDOT:PSS hybrid conductive particles with silver cores and polythiophene shells that can be used to formulate sinter-free inks for printing electronics. First, Ag nanocrystals capped with the weakly bound ligand aminohexanoic acid (ε-Ahx) are prepared. The ligand shell is exchanged by reacting the dispersion with the polymer ionomer mixture poly(3,4-ethylene dioxythiophene):polystyrene sulfonate (PEDOT:PSS). The particles are characterized by electron microscopy, dynamic light scattering, *Z* potential, and Raman spectroscopy, confirming the replacement of the ligands on the metal particle surface. The resulting dispersion is colloidally stable as confirmed by DLS. Inks with a solid content of the hybrid particles of 300 mg mL^{-1} were prepared and deposited on different substrates. The new particles are components for hybrid inks that become electrically conductive without any chemical or thermal post-deposition treatment. We show that silver-based hybrid inks can be deposited on different substrates and possess an average conductivity after 24 h of drying at room temperature of 1.726×10^6 S $m^{-1} \pm 0.326 \times 10^6$ S m^{-1}, only one order of magnitude lower than elemental silver and within the same order of magnitude as their gold ink counterpart.

Received 26th December 2022,
Accepted 21st January 2023

DOI: 10.1039/d2qi02722d

rsc.li/frontiers-inorganic

1. Introduction

Functional printing is an alternative material deposition strategy to build components in electronics. Printed devices include flexible and bendable displays,[1–3] touch panels,[4] light-emitting diodes and photovoltaic cells,[4] memory devices,[5] biosensors,[6] among others. Functional inks that yield electronic layers often contain colloidal metal nanoparticles (NPs). The resulting metal layers have higher conductivities than conductive polymers.[7–9]

Synthetic routes often yield metal NPs with bulky organic ligands that are electrically insulating and form tunnelling barriers between metal particles after drying.[10,11] Post-deposition treatments are used to remove them and improve electron transport between particles. Thermal sintering can remove the shell and connect the metallic cores, but its temperature requirements limit the choice of the substrate. Elevated temperatures and ligand removal can cause volume shrinkage, leading to cracks in printed structures.[12]

Hybrid NPs consisting of a gold core and a conductive organic shell avoid such problems. We have shown that the conductive polymers poly(3,4-ethylenedioxythiophene):polystyrene sulfonate (PEDOT:PSS) and poly[2-(3-thienyl)-ethyloxy-4-butylsulfonate] (PTEBS) simultaneously function as ligands that lend stability to gold–polymer hybrid nanoparticles and yield electrically conductive interfaces, thus obviating post-treatment.[13] Gold as core material provides high electronic conductivity and chemical stability. It has affinity for sulphur, making it possible to replace initial ligands with thiol bearing conductive polymers. The conductive polymers bind to the gold surface both *via* thiol and sulphonate groups of PTEBS. Commercial PEDOT:PSS (a mixture of conjugated polythiophene and sulfonated polystyrene) is an economically favourable alternative, and PEDOT:PSS covered gold NPs have shown higher electrical conductivities than those with PTEBS.[14]

Silver is a cheaper alternative to gold as core material with a bulk conductivity that surpasses that of gold. Here, we investigate the synthesis and properties of AgNPs@PEDOT:PSS hybrid particles. We therefore synthesized silver nanocrystals using a "sacrificial" ligand that binds strong enough to provide good morphological control but can be replaced by the

[a]*INM – Leibniz Institute for New Materials, Campus D2 2, D-66123 Saarbrücken, Germany. E-mail: alberto.escudero@csic.es, Tobias.Kraus@leibniz-inm.de*
[b]*Departamento de Química Inorgánica and Instituto de Investigaciones Químicas (IIQ), Universidad de Sevilla – CSIC, Calle Américo Vespucio 49, E-41092 Seville, Spain*
[c]*Department of Materials Science and Engineering, Saarland University, Campus D2 2, 66123 Saarbrücken, Germany*
[d]*Colloid and Interface Chemistry, Saarland University, D-66123 Saarbrücken, Germany*

† Electronic supplementary information (ESI) available. See DOI: https://doi.org/10.1039/d2qi02722d

functional ligand in a subsequent step, following a strategy previously realized for AuNPs@PEDOT:PSS.[14,15]

Silver nanoparticle syntheses have been described extensively in literature.[16] Common aqueous routes starting from precursors such as silver nitrate use sodium citrate[17] and polyvinylpyrrolidone (PVP)[18,19] as reducing and capping agents, which can also be combined.[20] Neither is suitable as sacrificial ligand for hybrid AgNP@PEDOT:PSS, however. Citrate ligands are easy to replace with thiol/sulphur-bearing ligands,[21] but the particle concentration is too low for functional inks. The low solubility of silver citrate implies typical Ag(I) concentrations around 0.25 mM to avoid silver citrate precipitation.[17] This results in few mg of AgNPs per laboratory-scale synthesis, while printing electronic applications require high NP concentration (typically several mL of 20–25 wt% dispersions for inkjet printing).[22] PVP allows higher silver precursor concentrations and usually yields stable dispersions, but the strong interaction between PVP and the silver surface through the nitrogen atom and carbonyl group on the pyrrolidine ring[23–25] restricts their exchange.[20,26]

Here, we show that aminohexanoic acid (ε-Ahx) is a suitable "sacrificial" capping ligand that can coordinate silver through its $-NH_2$ and –COOH functional groups.[27] It has been used as ligand for metal oxides and sulphides[28,29] and provides control of the NP morphology. We developed and optimized a polyol-based route[30] to homogeneous, hydrophilic, and colloidally stable AgNP@ε-Ahx with a mean core diameter of 82 ± 39 nm. Amounts around 1 g of AgNPs@ε-Ahx were obtained for a reaction volume of 200 mL. The conductive polymer PEDOT:PSS replaced ε-Ahx, as indicated by Raman measurements, and yielded AgNP@PEDOT:PSS that can be dispersed in water. Complete replacement of ligands was confirmed with Raman spectroscopy. The presence of PEDOT:PSS provided the hybrid NPs with good colloidal stability in water and good electron transport in a dry state. Finally, we show how these suspensions can be deposited onto different surfaces such as glass, PET, and Si wafer, yielding conductive structures just after drying at room temperature.

2. Experimental

2.1 Materials

All materials were used without further purification. Silver nitrate ($AgNO_3$, >99%), 6-aminohexanoic acid (ε-Ahx, ≥98.5%), sodium bromide (NaBr, >99%), and ethylene glycol (EG, 99.8%) were purchased from Sigma-Aldrich (Steinheim, Germany). Poly(3,4-ethylenedioxythiophene):polystyrene sulfonate (PEDOT:PSS, Clevios™ P) (aqueous dispersion) was purchased from Heraeus Deutschland GmbH & Co. KG (Leverkusen, Germany). Ultrapure water (*i.e.* water purified with a Millipore unit, ρ = 18.2 MΩ cm at 25 °C) was used for all syntheses, during ligand exchange, and in the cleaning steps. Components (Sylgard™ 184 Elastomer Base and Curing Agent) for preparing polymethylsiloxane (PDMS) molds were purchased from Dow Europe (Wiesbaden Germany). Silver paste (G3692) was purchased from Plano GmbH (Wetzlar, Germany).

2.2 Synthesis of hybrid AgNP@PEDOT:PSS

2.2.1 Synthesis of AgNP@ε-Ahx. Aminohexanoic-capped Ag NPs were synthesised by aging solutions of silver nitrate in EG at 80 °C in presence of ε-Ahx, H_2O and NaBr. We performed a systematic study to obtain homogeneous and colloidally stable AgNP@ε-Ahx. To do so, we varied the following synthetic parameters: ε-Ahx concentration, EG : H_2O ratio, and NaBr concentration, and studied their effect on the particle size and homogeneity as well as on their colloidal stability. The synthesis is described below for sample Ag11, which showed the smallest core size and better homogeneity and colloidal stability; the conditions for all samples are summarized in Table 1.

Table 1 Experimental conditions for different AgNP@ε-Ahx syntheses. All particles formed at a concentration of 88 mM $AgNO_3$ (15 mg mL^{-1}, 88 mM) in sealed tubes at 80 °C during 5 h. Particle sizes observed by DLS, and SEM are also given

Sample name	EG (mL)	H_2O (mL; total vol%)	[ε-Ahx] (mg mL^{-1})	128 mM NaBr (μL)/Br : Ag molar ratio	Hydrodynamic diameter (nm)	*Z*-Average (nm)	Core size (SEM) ($x \pm \sigma$, nm)
Ag1	10.00	0.0	0.0	0	n.a.	n.a.	n.a.
Ag2	10.00	0.0	11.1	0	396	246	130 ± 97
Ag3	10.00	0.0	22.2	0	342	350	237 ± 159
Ag4	10.00	0.0	27.8	0	615	718	209 ± 139
Ag5	9.00	1; 10%	11.1	0	295	241	250 ± 208
Ag6	9.50	0.5; 5%	11.1	0	295	222	239 ± 127
Ag7	9.75	0.25; 2.5%	11.1	0	220	187	146 ± 67
Ag8	9.90	0.1; 1%	11.1	0	220	231	168 ± 96
Ag9	9.75	0.236; 2.5%	11.1	14/0.002	190	146	92 ± 47
Ag10	9.75	0.215; 2.5%	11.1	64.5/0.005	220	162	138 ± 73
Ag11	9.75	0.181; 2.5%	11.1	69/0.01	142	114	85 ± 33
Ag12	9.75	0.112; 2.5%	11.1	138/0.02	190	149	106 ± 67
Ag13	195	3.62; 2.5%	11.1	138/0.01	142	121	82 ± 39
Ag13 LE	Ligand exchange of Ag13 with PEDOT:PSS				190	191	100 ± 44

Aminohexanoic acid (ε-Ahx) (111 mg) was dissolved in a mixture of EG : H_2O (9.75 mL : 0.181 mL) at 50 °C under stirring. The solution was cooled to room temperature, and 69 μL of a 128 mM NaBr solution (total added H_2O 0.250 mL, 2.5 vol%) and solid $AgNO_3$ (150 mg) were added under stirring. The final $AgNO_3$ concentration was thus 15 mg mL^{-1} or 88 mM. After complete dissolution of the reactants, the reaction mixture was transferred to sealed tubes (culture vials with screw cap DURAN® glass, DWK Life Sciences) and placed in an oven at 80 °C for 5 h. The tubes were removed, left to cool to room temperature, and the resulting suspensions were centrifuged (7450 rcf, 45 min) to sediment the dispersed particles. The supernatants were removed, the centrifuge tubes were refilled with ethanol, and the suspension was sonicated in a bath for 20–30 min. This process was repeated three times using ultrapure water as a solvent. The particles were finally dispersed in ~5 mL of ultrapure water.

This synthesis protocol for sample Ag11 was scaled up to a reaction volume of at 200 mL at unchanged reagent concentrations, which yielded approximately 1 g of AgNP@ε-Ahx. In particular, sample Ag13, was prepared in a glass reagent bottle (Simax, Kavalierglass, CZ) equipped with a screw cap at 50 °C under stirring by dissolving 2.22 g of aminohexanoic acid (ε-Ahx) in a mixture consisting of 195 mL of EG and 3.62 mL of ultrapure H_2O. After complete dissolution and cooling down at room temperature, 1.38 mL of 128 mM NaBr and 3 g of solid $AgNO_3$ were added and dissolved under stirring, and the closed bottle was placed in the oven at 80 °C for 5 h. After synthesis, the obtained suspensions were centrifuged as described previously, and the final obtained particles were dispersed in around 40 mL of ultrapure water (approx. 30 mg mL^{-1} solid content).

2.2.2 Ligand exchange with PEDOT:PSS to obtain hybrid AgNP@PEDOT:PSS. The ligand exchange was performed on the Ag13 sample, which consisted of AgNP@ε-Ahx dispersed in around 40 mL of ultrapure water with a solid concentration of 30 mg mL^{-1}. The sacrificial ligand was replaced by incubating the AgNP@ε-Ahx with PEDOT:PSS dispersion for 48 h at room temperature. A 1 : 1 wt% NP : polymer ratio was achieved by adding 93 mL of Clevios P solution (1.3 wt% PEDOT:PSS) to the Ag13 sample. The total volume was thus 133 mL at an NP concentration of approximately 9 mg mL^{-1}. After 48 h under stirring, the dispersion was centrifuged (7450 rcf, 45 min), as much as possible of the supernatant was removed, and the sediment was washed once with ethanol and four times with ultrapure water (see Section 2.2.1). The aqueous dispersion was finally concentrated by centrifugation (7450 rcf, 45 min) to obtain 3 mL at a final concentration of 300 mg mL^{-1}, resulting in sample Ag13LE. The total yield in terms of silver mass after core synthesis, ligand exchange, and all centrifugation steps was approximately 80%.

2.3 Nanoparticle characterization

2.3.1 Dynamic light scattering. Distributions of the hydrodynamic diameter of suspensions of AgNP@ε-Ahx and AgNP@PEDOT:PSS in water were determined using dynamic light scattering (DLS) with a Malvern Nano ZSP Zetasizer with a laser wavelength of 632.8 nm. Dispersions were measured in disposable poly(methyl methacrylate) (PMMA) cuvettes at a constant silver particle concentration of 1 mg mL^{-1} in 1.5 mL sample volume. All measurements were performed at 25 °C. Hydrodynamic diameters were calculated from DLS autocorrelations using the instrument software, and the *z*-average diameters were obtained using a cumulant analysis. The ζ potentials of NP suspensions in water at pH 6.5 were measured in the same setup using the built-ion Doppler-based electrophoresis analysis.

2.3.2 Inductively coupled plasma atomic emission spectroscopy. The silver concentrations of the resulting suspensions were assessed by concentration measurements *via* inductively couples plasma atomic emission spectroscopy (ICP-AES) using an ICP Horiba Jobin Yvon ULTIMA2 spectrometer. The silver NPs were first dissolved at room temperature in the minimum possible amount of HNO_3.

2.3.3 Electron microscopy. Scanning electron microscopy (SEM) micrographs of drop cast samples of AgNP@ε-Ahx and AgNP@PEDOT:PSS particles on a silicon wafer were recorded with a Quanta 400 ESEM (FEI, Germany) at 10 kV acceleration voltage using a secondary electron detector. Particle size and size distributions were obtained from the SEM micrographs by measuring the diameters of the smallest inscribing circle for each particle, and calculated their mean and standard deviations. To do so, we counted approximately one hundred particles. Transmission electron microscopy (TEM) measurements were performed using a JEM-2100 transmission electron microscope from JEOL (Germany) with an acceleration voltage of 200 kV. EDX analysis was performed using Noran System 7 X-ray Microanalysis System (Thermo Scientific). For TEM sample preparation, 2 μL of a diluted particle suspension were dried on a carbon-coated copper grid.

2.3.4 Raman spectroscopy. Samples were prepared by depositing aqueous AgNP@ε-Ahx and AgNP@PEDOT:PSS dispersions onto steel substrates. The dried films were analysed using a confocal Raman microscope inVia (Renishaw, United Kingdom). The excitation wavelength of the used laser was 633 nm for both AgNP@ε-Ahx and AgNP@PEDOT:PSS samples.

2.3.5 X-ray diffractometry. A Bruker AXS (Karlsruhe, Germany) D8 Advance X-ray diffractometer equipped with a Lynxeye detector and Cu Kα spectral line source was used in theta/2theta geometry to collect the X-ray reflections. The data was analysed using Topas analysis software (Bruker AXS, Karlsruhe, Germany).

2.4 Electrical characterization

Deposition was tested and electrical properties were measured using AgNP@PEDOT:PSS particles from sample Ag13LE, which was the upscaled sample obtained from Ag cores showing the smallest size, narrow size distribution, and minimal degree of aggregation. The solid content was 300 mg mL^{-1}. Well-defined lines were drop-cast on glass with the aid of PDMS moulds that had an opening of 0.1 cm. Ink was de-

posited 5 times and dried at room temperature for 15 min after each step. This resulted in rectangular films that were 0.9 ± 0.03 cm long and 0.09 ± 0.02 cm wide. The exact lateral dimensions of the deposited films were determined using an Olympus microscope SZX16 (Olympus, Japan). The thickness was determined using a 3D confocal microscope MarSurf CM explorer (Mahr, Germany). Their topography was converted to histograms and fitted by Gaussian functions to obtain the mean thickness of 5.3 ± 0.5 μm. The ends of the deposited lines were coated with silver paste, which served as robust electrical contacts with low resistance that were connected to a 2450 Sourcemeter (Keithley Instruments, Ohio, USA) using a 2-point probe setup. The current at voltages between −25 mV and 25 mV was measured for a total of 10 samples. The material resistivity was calculated according to eqn (1):

$$\rho = R \cdot t \cdot \frac{w}{l} \quad (1)$$

in equation, ρ is resistivity, R is resistance in Ω, t, w and l are thickness, width, and film length, respectively. Additional layers were prepared by using a fountain pen that was loaded with AgNP@PEDOT:PSS ink (300 mg mL^{-1}) on glossy paper as substrate. A light-emitting diode (LED) and batteries were connected to the circuit with silver paste as shown in Fig. 5C.

3. Results and discussion

Silver nanocrystals with defined morphology and the sacrificial ligand ε-Ahx were prepared and the ligand was replaced with the conductive polymer PEDOT:PSS. Section 3.1 discusses the preparation of homogenous and colloidally stable AgNP@ε-Ahx. Section 3.2 focuses on the ligand exchange towards AgNP@PEDOT:PSS. The colloidal stability of the hybrid particles is described in Section 3.3, and the deposition of the hybrid particles and the electrical characterization of their films is covered in Section 3.4.

3.1 AgNP@ε-Ahx synthesis

In general terms, the smaller size and uniform dispersion of silver nanoparticles in inks make them suitable for printing, with typical nanoparticle sizes below 200 nm.[22] We modified a polyol route to synthesize AgNP@ε-Ahx with this suitable size, morphology, and colloidal stability that could be later converted in conductive AgNP@PEDOT:PSS. The original polyol strategy for the synthesis of AgNP consists of reducing the metal precursor by a polyol, which also acts as a solvent, in the presence of an appropriate capping agent, usually polyvinylpyrrolidone (PVP), at moderated temperatures (80–150 °C).[31,32] Given that PVP shows a high affinity toward the AgNP surface,[33] it is unsuitable for subsequent ligand exchange. We retained ethylene glycol as reducing solvent but used aminohexanoic acid (ε-Ahx), a derivative of the amino acid lysine, as a "sacrificial" and morphology-directing ligand, and optimized the ligand concentration, solvent composition, ionic strength, and other variables to obtain small and homogeneous particles. All syntheses were performed at 88 mM (15 mg mL^{-1}) $AgNO_3$ in 10 mL synthesis volumes. A summary of the performed variations in synthesis conditions is shown in Table 1.

First, we investigated the effect of ε-Ahx ligand concentration on particle synthesis. Aging solutions of $AgNO_3$ in pure EG at 80 °C in the absence of ε-Ahx produced large (>1 μm) and polydisperse particles (sample Ag1, Fig. 1A). Addition of ε-Ahx at 11.1 mg mL^{-1} yielded smaller, less aggregated, and less polydisperse particles with a mean core diameter of 130 ± 97 nm and a mean hydrodynamic diameter of 396 nm, as determined from scanning electron microscopy (SEM) images and dynamic light scattering (DLS) analyses, respectively (sample Ag2, Fig. 1B). Increasing the ε-Ahx concentration to 22.1 and 27.7 mg mL^{-1} (samples Ag3 and Ag4, respectively) produced larger and more polydisperse particles with core diameters of 237 ± 159 nm and 209 ± 139 nm (Fig. S1C and D†). The large difference in between hydrodynamic diameters of the particles and their core size determined from SEM indicated particle aggregation in water. The smallest and most homogeneous particles were obtained at a ε-Ahx concentration of 11.1 mg mL^{-1}; they exhibited some agglomeration (sample Ag2).

We further modified the synthesis based on sample Ag2 and added small amounts of water to narrow the particle size dispersion and improve their colloidal stability (*i.e.*, reduce the

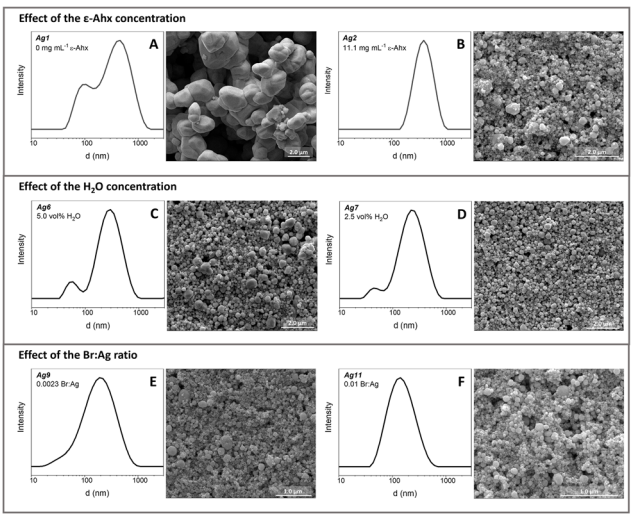

Fig. 1 SEM images and DLS data of the resulting silver particles obtained after a systematic variation of the synthesis conditions. (A) AgNP prepared in EG in the absence of ε-Ahx (sample Ag1); (B) AgNP@ε-Ahx prepared in EG in the presence of ε-Ahx, concentration 11.1 mg mL^{-1} (sample Ag2); (C) AgNP@ε-Ahx, prepared in EG/H_2O (5 vol% H_2O) in the presence of ε-Ahx, concentration 11.1 mg mL^{-1} (sample Ag6); (D) AgNP@ε-Ahx, prepared in EG/H_2O (2.5 vol% H_2O) in the presence of ε-Ahx, concentration 11.1 mg mL^{-1} (sample Ag7); (E) AgNP@ε-Ahx, prepared in EG/H_2O (2.5 vol% H_2O) in the presence of ε-Ahx (11.1 mg mL^{-1}) and NaBr (Br : Ag, 0.0023, sample Ag9); (F) AgNP@ε-Ahx, prepared in EG/H_2O (2.5 vol% H_2O) in the presence of ε-Ahx (11.1 mg mL^{-1}) and NaBr (Br : Ag, 0.01, sample Ag11). Optimizing of the ε-Ahx, and water and NaBr amounts yielded smaller, more homogeneous, and more colloidally stable AgNP@ε-Ahx.

level of particle aggregation). For many polyol syntheses, this strategy has been reported to introduce a change in viscosity and dielectric constant and a change in reaction kinetics.[34,35] The effect of water is associated with reduced viscosity and dielectric constant of the reaction media that affects reaction kinetic and colloidal stability.[36,37] The addition of >5 vol% of water (samples Ag5 and Ag6) did not affect the core particle size and did not reduce polydispersity (Fig. 1C for sample Ag6, and Fig. S2A and B†). However, it did reduce the level of aggregation, as indicated by the hydrodynamic diameters being more similar to the core sizes determined from their SEM images. The addition of 2.5 vol% of H_2O (sample Ag7) reduced the core diameter to 146 ± 67 nm (Fig. 1D) and the hydrodynamic diameter to 220 nm (*Z* average size 187 nm). The addition of 1 vol% water (sample Ag8, Fig. S2D) resulted in a similar value for the hydrodynamic diameter and in a slightly larger core size.

We added small amounts of NaBr solutions to the protocol used in the sample Ag7. It is known that oxidative etching plays a significant part in regulating the crystallinity and geometry of many metal nanocrystals. This strategy alters the types and distributions of products produced during the nucleation and growth processes by oxidizing zerovalent metal species to their ionic state.[38] The presence of air and halides like Cl^- and Br^- during polyol synthesis of silver particles induces partial dissolution of the particles initially formed. As a result, the nucleation and growth are delayed, and particle size and morphology change.[38–42]

The syntheses of samples Ag9–Ag12 (Fig. 1E for sample Ag9, and Fig. S3†) were performed while varying the Br : Ag ratio from 0.0023 to 0.02. The shape of the resulting AgNP@ε-Ahx was unchanged according to SEM, but core diameters and hydrodynamic diameters in aqueous dispersions were reduced. In particular, sample Ag11 (Fig. 1F) had a core diameter of 85 ± 33 nm, a mean hydrodynamic diameter of 142 nm (*Z* average size 114 nm) indicating slight aggregation, and a ζ-potential of −16 mV.

Among all the synthesized AgNP@ε-Ahx, sample Ag11, synthesized in the presence of 11.1 mg mL^{-1} ε-Ahx, 2.5 vol% water, and a 0.01 Br : Ag molar ratio, provided the optimal particle size with a narrower size distribution and minimal degree of aggregation and was most suitable for inkjet inks. We scaled the protocol to create AgNP@ε-Ahx in larger volumes up to 200 mL (sample Ag13) and found that the same parameters yielded very similar particles as at 10 mL (Table 1).

3.2 Surface modification by ligand exchange with PEDOT:PSS

The ε-Ahx shell of the particles in sample Ag13 was replaced by the conductive polymer PEDOT:PSS to obtain hybrid AgNP@PEDOT:PSS (sample Ag13LE). The original dispersion was incubated with an aqueous PEDOT:PSS dispersion at 1 : 1 mass ratio polymer : silver in a total reaction volume of 133 mL. The conditions were similar to those reported for AuNP@PEDOT:PSS by ligand exchange from AuNP@CTAB.[14] The total loss of silver during synthesis and purification was approximately 20%.

The presence of aminohexanoic acid on the surface of the particles in sample Ag13 was confirmed by Raman spectroscopy (Fig. 2B). The strongest peak at 1418 cm^{-1} was assigned to the symmetrical stretching mode of carboxylate groups (ν_s COO^-). This observation indicates that the carboxyl group of ε-Ahx is ionized and interacts with the metal surface.[43] The strong peak at 1606 cm^{-1} was assigned to the deformation of the amino group ($-NH_2$). This peak is very weak in the Raman spectrum of pristine ε-Ahx (Fig. 2A) but it is enhanced and shifted towards higher wavelengths (1625 cm^{-1}) due to surface enhanced Raman scattering in presence of silver.[43,44] The observed changes in peak intensity and shift indicate a possible bonding between the metal and the amino end group side. Finally, bands at 2800–2900 cm^{-1} were assigned to the frequency of NH_2 stretching and the vibrational modes of –OH from water, and the peak at 1442 cm^{-1} was assigned to the bending vibrations of CH_2 groups.[44]

The Raman spectrum of the particles after ligand exchange (Ag13LE sample) in Fig. 2D shows the characteristic bands of pure PEDOT:PSS (compare Fig. 2C). Peaks appearing at 1363, 1424, 1533, and 1566 cm^{-1} were assigned to the vibrational stretching modes of the thiophene ring, and the peak at 1258 cm^{-1} was assigned to the stretching of the bonds between two thiophene rings.[45,46] Peaks in the region 400–1000 cm^{-1} corresponded to the deformation of the ethylenedioxy and thiophene rings.[47] The vibrational modes of the thiophene ring stretching were enhanced in the spectrum of the AgNP@PEDOT:PSS (Fig. 2D), and the strongest peak appeared at 1538 cm^{-1}. Enhancement of peaks in the 950–1150 cm^{-1} region likely is a result of desulfonation of PSS and/or oxidative addition to the sulphur atom, and is consistent with previous studies on PEDOT:PSS in the presence of silver.[45,48] This, and the absence of the prominent ε-Ahx peaks assigned to carboxylate group (1418 cm^{-1}) and amino group (1606 cm^{-1}) (Fig. 2B), confirms the presence of PEDOT:PSS on

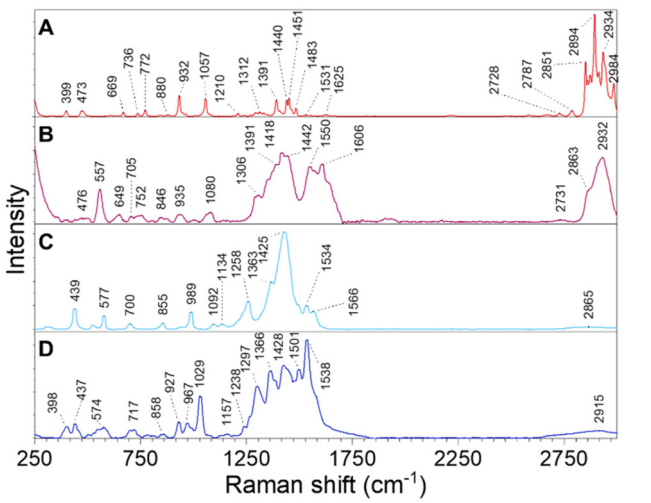

Fig. 2 Raman spectra of (A) pristine ε-Ahx; (B) AgNP@ε-Ahx, sample Ag11; (C) pristine PEDOT:PSS and (D) AgNP@PEDOT:PSS nanoparticles.

the AgNP surface and the replacement of the original "sacrificial" ligand by PEDOT:PSS.

We observed no morphological changes in particles after the ligand exchange, as shown in Fig. 3A and B (before and after ligand exchange). The particles kept a similar particle size and size distribution and retained their quasi-spherical shape. The ζ-potential decreased from −16 to −35 mV after ligand exchange. Nanoparticles with ζ-potential greater than +30 mV and −30 mV are often considered "stable".[49] The mean hydrodynamic diameter increased from 142 to 190 nm (Fig. 3D), probably due the presence of a PEDOT:PSS shell around the silver core.

Silver particles tend to oxidize at their surface. The presence of an oxide layer may change optical and electrical properties, limiting their applicability. In particular, when the aim is to produce sinter-free inks for printed electronics, oxidation of metal can lower overall electrical conductivity of the material. We investigated the oxidation state of the particles after ligand exchange. The XRD of sample AgNP@PEDOT:PSS (Fig. 3E) shows the expected signals of crystalline silver (JCPDS file no. 04-0783) and no signs of silver oxide (Ag_2O). The EDX spectrum (Fig. 3F) only shows Ag and Br, but no oxygen. The limit of detection for oxygen is approximately 0.5 at%; oxidation during synthesis and ligand exchange was thus limited. Transmission electron microscopy did not indicate lower density-shells around the particles that may indicate oxidation (Fig. 3C).

3.3 Colloidal stability and sedimentation of AgNP@PEDOT:PSS

The colloidal stability of AgNP@PEDOT:PSS was studied by monitoring the hydrodynamic diameter over time. Samples were diluted with ultrapure water to 1 mg mL^{-1} and stored at room temperature in gas-tight vessels. After five days, the mean hydrodynamic diameter of 190 nm had not changed (Fig. 4A). Sedimentation occurred as expected (Fig. 4B), but the particles could be successfully redispersed and were successfully deposited to form conductive layer almost 2 years post synthesis.

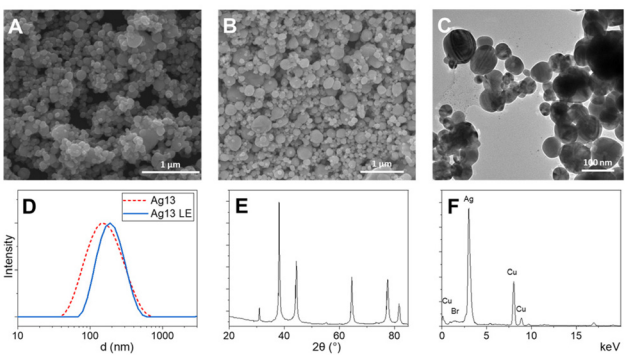

Fig. 3 (A) SEM micrograph of sample Ag13 (AgNP@ε-Ahx); (B and C) SEM and TEM images of sample Ag13LE (AgNP@PEDOT:PSS); (D) DLS spectra of sample Ag13 (AgNP@ε-Ahx, red dotted line) and Ag13LE (AgNP@PEDOT:PSS, blue line); (E) XRD spectra of sample Ag13LE (AgNP@PEDOT:PSS); (F) EDX spectra of sample Ag13LE (AgNP@PEDOT:PSS).

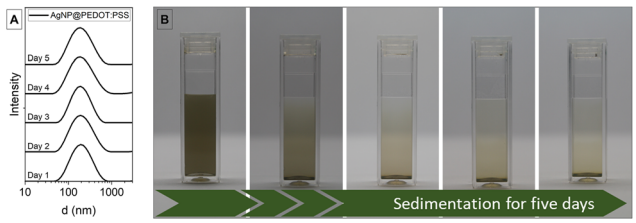

Fig. 4 (A) Hydrodynamic diameter of AgNP@PEDOT:PSS determined by DLS, showing stability for 5 days; (B) visible sedimentation of redispersed diluted AgNP@PEDOT:PSS dispersions.

3.4 Deposition and electrical characterization of conductive AgNP@PEDOT:PSS

The concentrated aqueous dispersion of the hybrid AgNP@PEDOT:PSS (300 mg mL^{-1}, sample Ag13LE, Section 2.2.2) was deposited on glass with a stencil mask (see Section 2.4 in Experimental section) to create conductive films. The films became conductive after drying at room temperature. Reference films prepared from AgNP@ε-Ahx particles in the same way had no measurable conductivity after drying. Typical *I–V* curves of AgNP@PEDOT:PSS films one hour after deposition are shown in Fig. 5A. A specific conductivity of $3 \times 10^3 \pm 6 \times 10^3$ S m^{-1} was calculated using eqn (1) at a thickness of 5.5 ± 0.5 µm (see Experimental section). This conductivity is three orders of magnitude below that reported for AgNP-based inkjet inks after sintering at 100–400 °C for at least 30 min to two hours[50–55] but above that reported for dry PEDOT:PSS films (0.02–0.2 S m^{-1} [56]). Resistance measurements were repeated 24 h after deposition and calculated average conductivity was 1.7×10^6 S $m^{-1} \pm 0.3 \times 10^6$ S m^{-1}. The silver-based material is half as conductive as hybrid gold nanorod ink with the same ligand (AuNR@PEDOT:PSS)[14] reported previously.

The silver-based hybrid particles are applicable for the formulation of water-based, low-viscosity inks for functional printing. Printed layers are mechanically flexible. A basic demonstration of the applicability on standard substrates is shown in Fig. 5. We used a simple pen in which our concentrated aqueous dispersion of AgNP@PEDOT:PSS (sample Ag13LE)

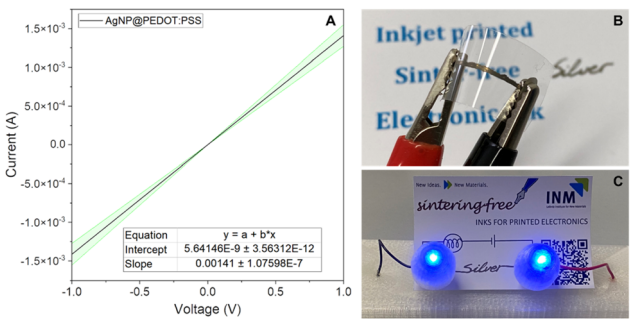

Fig. 5 (A) Voltage–current curve measured on deposited AgNP@PEDOT:PSS; (B) image of AgNP@PEDOT:PSS deposited on bendable substrate (PET); (C) image of deposited AgNP@PEDOT:PSS on paper and connected into a circuit with LEDs and power source.

was used as an ink to deposit lines PET foils (Fig. 5B) and photopaper (Fig. 5C).

4. Conclusions

We have developed a two-step protocol to synthesize stable, hybrid conductive particles consisting of a silver core and a conductive PEDOT:PSS shell. The strategy comprised synthesizing morphology-controlled homogenous AgNP@ε-Ahx followed by ligand exchange with the electrically conductive polymer PEDOT:PSS. The synthesis was performed in ethylene glycol, and the procedure was optimized to obtain homogenous AgNP@ε-Ahx with a mean hydrodynamic diameter of 142 nm by adding small amounts of water and NaBr. In a second step, ligand exchange was performed in water with PEDOT:PSS and confirmed by Raman spectroscopy, yielding a stable hybrid AgNP@PEDOT:PSS. Finally, concentrated dispersions of such hybrid NPs were deposited on the glass substrate to form conductive structures upon drying at room temperature without additional post-deposition treatments.

Author contributions

Concept and funding acquisition, T. K.; investigation, J. D., and A. E.; supervision, T. K., A. E.; L. G.-G.; writing—original draft, J. D., and A. E.; writing—review & editing, J. D.; A. E.; L. G.-G., and T. K.

Conflicts of interest

The authors declare that they have no known competing financial interests or personal relationships that could have appeared to influence the work reported in this paper.

Acknowledgements

The authors thank Anna Zimmerman and Indra Backes for TEM/EDX and Raman measurements of silver nanoparticles, respectively, Michael Klos for help with some DLS measurements, Petra Herbeck-Engel for XRD measurements, and Dominik Perius for additional conductivity calculations and measurements of deposited silver nanoparticle films. A. E. also acknowledges the support of the sixth Research and Technology Transfer Plan of the University of Seville (VI PPIT-US).

Notes and references

1 M. Leufgen, A. Lebib, T. Muck, U. Bass, V. Wagner, T. Borzenko, G. Schmidt, J. Geurts and L. W. Molenkamp, Organic thin-film transistors fabricated by microcontact printing, *Appl. Phys. Lett.*, 2004, **84**, 1582–1584.
2 O. Kina, M. Koutake, K. Matsuoka and K. Yase, Organic thin-film transistors fabricated by microcontact printing, *Jpn. J. Appl. Phys.*, 2010, **49**, 1–07.
3 L. Zhang, C. A. Di, G. Yu and Y. Liu, Solution processed organic field-effect transistors and their application in printed logic circuits, *J. Mater. Chem.*, 2010, **20**, 7059–7073.
4 S. Takamatsu, T. Takahata, M. Muraki, E. Iwase, K. Matsumoto and I. Shimoyama, Transparent conductive-polymer strain sensors for touch input sheets of flexible displays Related content, *J. Micromech. Microeng.*, 2010, **20**, 075017.
5 J. Leppäniemi, T. Mattila, T. Kololuoma, M. Suhonen and A. Alastalo, Roll-to-roll printed resistive WORM memory on a flexible substrate, *Nanotechnology*, 2012, **23**, 12.
6 A. Martínez-Olmos, J. Fernández-Salmerón, N. Lopez-Ruiz, A. Rivadeneyra Torres, L. F. Capitan-Vallvey and A. J. Palma, Screen printed flexible radiofrequency identification tag for oxygen monitoring, *Anal. Chem.*, 2013, **85**, 11098–11105.
7 T. Minari, Y. Kanehara, C. Liu, K. Sakamoto, T. Yasuda, A. Yaguchi, S. Tsukada, K. Kashizaki and M. Kanehara, Room-temperature printing of organic thin-film transistors with π-junction gold nanoparticles, *Adv. Funct. Mater.*, 2014, **24**, 4886–4892.
8 K. Woo, C. Bae, Y. Jeong, D. Kim and J. Moon, Inkjet-printed Cu source/drain electrodes for solution-deposited thin film transistors, *J. Mater. Chem.*, 2010, **20**, 3877–3882.
9 J.-H. Jou, P.-Y. Hwang, W.-B. Wang, C.-W. Lin, Y.-C. Jou, Y.-L. Chen, J.-J. Shyue, S.-M. Shen and S.-Z. Chen, High-efficiency low color temperature organic light emitting diodes with solution-processed emissive layer, *Org. Electron.*, 2012, **13**, 899–904.
10 S. Wünscher, R. Abbel, J. Perelaer and U. S. Schubert, Progress of alternative sintering approaches of inkjet-printed metal inks and their application for manufacturing of flexible electronic devices, *J. Mater. Chem. C*, 2014, **2**, 10232–10261.
11 M. A. Boles, D. Ling, T. Hyeon and D. V. Talapin, The surface science of nanocrystals, *Nat. Mater.*, 2016, **15**, 141–153.
12 J. Y. Y. Kim and N. A. A. Kotov, Charge transport dilemma of solution-processed nanomaterials, *Chem. Mater.*, 2014, **26**, 134–152.
13 D. J. Kang, Y. Jüttke, L. González-García, A. Escudero, M. Haft and T. Kraus, Reversible Conductive Inkjet Printing of Healable and Recyclable Electrodes on Cardboard and Paper, *Small*, 2020, **16**, 2000928.
14 B. Reiser, L. González-García, I. Kanelidis, J. H. M. Maurer and T. Kraus, Gold nanorods with conjugated polymer ligands: Sintering-free conductive inks for printed electronics, *Chem. Sci.*, 2016, **7**, 4190–4196.
15 A. Escudero, L. Gonzalez-Garcia, R. Strahl, D. J. Kang, J. Drzic and T. Kraus, Large-Scale Synthesis of Hybrid Conductive Polymer-Gold Nanoparticles Using "sacrificial" Weakly Binding Ligands for Printing Electronics, *Inorg. Chem.*, 2021, **60**, 17103–17113.
16 A. Heuer-Jungemann, N. Feliu, I. Bakaimi, M. Hamaly, A. Alkilany, I. Chakraborty, A. Masood, M. F. Casula,

A. Kostopoulou, E. Oh, K. Susumu, M. H. Stewart, I. L. Medintz, E. Stratakis, W. J. Parak and A. G. Kanaras, The role of ligands in the chemical synthesis and applications of inorganic nanoparticles, *Chem. Rev.*, 2019, **119**, 4819–4880.

17 N. G. Bastús, F. Merkoçi, J. Piella and V. Puntes, Synthesis of highly monodisperse citrate-stabilized silver nanoparticles of up to 200 nm: Kinetic control and catalytic properties, *Chem. Mater.*, 2014, **26**, 2836–2846.

18 Y. Sun and Y. Xia, Shape-controlled synthesis of gold and silver nanoparticles, *Science*, 2002, **298**, 2176–2179.

19 X. Xia, J. Zeng, L. K. Oetjen, Q. Li and Y. Xia, Quantitative analysis of the role played by poly(vinylpyrrolidone) in seed-mediated growth of Ag nanocrystals, *J. Am. Chem. Soc.*, 2012, **134**, 1793–1801.

20 L. Rainville, M. C. Dorais and D. Boudreau, Controlled synthesis of low polydispersity Ag@SiO_2 core–shell nanoparticles for use in plasmonic applications, *RSC Adv.*, 2013, **3**, 13953–13960.

21 Á. I. López-Lorente, M. L. Soriano and M. Valcárcel, Analysis of citrate-capped gold and silver nanoparticles by thiol ligand exchange capillary electrophoresis, *Microchim. Acta*, 2014, **181**, 1789–1796.

22 L. Nayak, S. Mohanty, S. K. Nayak and A. Ramadoss, A review on inkjet printing of nanoparticle inks for flexible electronics, *J. Mater. Chem. C*, 2019, **7**, 8771–8795.

23 H. H. Huang, X. P. Ni, G. L. Loy, C. H. Chew, K. L. Tan, F. C. Loh, J. F. Deng and G. Q. Xu, Photochemical formation of silver nanoparticles in poly(N-vinylpyrrolidone), *Langmuir*, 1996, **12**, 909–912.

24 B. Yin, H. Ma, S. Wang and S. Chen, Electrochemical synthesis of silver nanoparticles under protection of poly(N-vinylpyrrolidone), *J. Phys. Chem. B*, 2003, **107**, 8898–8904.

25 Y. Gao, P. Jiang, D. F. Liu, H. J. Yuan, X. Q. Yan, Z. P. Zhou, J. X. Wang, L. Song, L. F. Liu, W. Y. Zhou, G. Wang, C. Y. Wang, S. S. Xie, J. M. Zhang and D. Y. Shen, Evidence for the monolayer assembly of poly(vinylpyrrolidone) on the surfaces of silver nanowires, *J. Phys. Chem. B*, 2004, **108**, 12877–12881.

26 S. Zhang, S. Kim and V. V. Tsukruk, Ligand-Exchange Dynamics on Gold Nanocrystals: Direct Monitoring of Nanoscale Polyvinylpyrrolidone-Thiol Domain Surface Morphology, *Langmuir*, 2017, **33**, 3576–3587.

27 T. D. Nguyen, D. Mrabet, T. T. D. Vu, C. T. Dinh and T. O. Do, Biomolecule-assisted route for shape-controlled synthesis of single-crystalline MnWO4 nanoparticles and spontaneous assembly of polypeptide-stabilized mesocrystal microspheres, *CrystEngComm*, 2011, **13**, 1450–1460.

28 J. D. Patel, F. Mighri, A. Ajji and S. Elkoun, Room Temperature Synthesis of Aminocaproic Acid-Capped Lead Sulphide Nanoparticles, *Mater. Sci. Appl.*, 2012, **03**, 125–130.

29 H. G. Jeong, B. G. Cha, D. W. Kang, D. Y. Kim, S. K. Ki, S. I. Kim, J. H. Han, W. Yang, C. K. Kim, J. Kim and S. H. Lee, Ceria nanoparticles synthesized with aminocaproic acid for the treatment of subarachnoid hemorrhage, *Stroke*, 2018, **49**, 3030–3038.

30 X. Wang, W. Guo, Y. Zhu, X. Liang, F. Wang and P. Peng, Electrical and Mechanical Properties of Ink Printed Composite Electrodes on Plastic Substrates, *Appl. Sci.*, 2018, **8**, 2101.

31 D. Kim, S. Jeong and J. Moon, Synthesis of silver nanoparticles using the polyol process and the influence of precursor injection, *Nanotechnology*, 2006, **17**, 4019–4024.

32 A. Escudero, C. Carrillo-Carrión, E. Romero-Ben, A. Franco, C. Rosales-Barrios, M. C. Castillejos and N. Khiar, Molecular Bottom-Up Approaches for the Synthesis of Inorganic and Hybrid Nanostructures, *Inorganics*, 2021, **9**, 58.

33 S. Zhang, S. Kim and V. V. Tsukruk, Ligand-Exchange Dynamics on Gold Nanocrystals: Direct Monitoring of Nanoscale Polyvinylpyrrolidone-Thiol Domain Surface Morphology, *Langmuir*, 2017, **33**, 3576–3587.

34 T. Inose, S. Toyouchi, G. Lu, K. Umemoto, Y. Tezuka, B. Lyu, A. Masuhara, E. Fron, Y. Fujita, K. Hirai and H. Uji-I, Water-mediated polyol synthesis of pencil-like sharp silver nanowires suitable for nonlinear plasmonics, *Chem. Commun.*, 2019, **55**, 11630–11633.

35 G. Hemery, A. C. Keyes, E. Garaio, I. Rodrigo, J. A. Garcia, F. Plazaola, E. Garanger and O. Sandre, Tuning Sizes, Morphologies, and Magnetic Properties of Monocore Versus Multicore Iron Oxide Nanoparticles through the Controlled Addition of Water in the Polyol Synthesis, *Inorg. Chem.*, 2017, **56**, 8232–8243.

36 N. Nuñez, J. Sabek, J. García-Sevillano, E. Cantelar, A. Escudero and M. Ocaña, Solvent-Controlled Synthesis and Luminescence Properties of Uniform Eu:YVO_4 Nanophosphors with Different Morphologies, *Eur. J. Inorg. Chem.*, 2013, 1301–1309.

37 A. Escudero, E. Moretti and M. Ocaña, Synthesis and luminescence of uniform europium-doped bismuth fluoride and bismuth oxyfluoride particles with different morphologies, *CrystEngComm*, 2014, **16**, 3274–3283.

38 Y. Zheng, J. Zeng, A. Ruditskiy, M. Liu and Y. Xia, Oxidative etching and its role in manipulating the nucleation and growth of noble-metal nanocrystals, *Chem. Mater.*, 2014, **26**, 22–33.

39 B. Wiley, T. Herricks, Y. Sun and Y. Xia, Polyol synthesis of silver nanoparticles: Use of chloride and oxygen to promote the formation of single-crystal, truncated cubes and tetrahedrons, *Nano Lett.*, 2004, **4**, 1733–1739.

40 B. J. Wiley, Y. Xiong, Z.-Y. Y. Li, Y. Yin and Y. Xia, Right bipyramids of silver: A new shape derived from single twinned seeds, *Nano Lett.*, 2006, **6**, 765–768.

41 H. I. Sang, T. L. Yun, B. Wiley and Y. Xia, Large-Scale Synthesis of Silver Nanocubes: The Role of HCl in Promoting Cube Perfection and Monodispersity, *Angew. Chem., Int. Ed.*, 2005, **44**, 2154–2157.

42 F. Wu, W. Wang, Z. Xu and F. Li, Bromide (Br) – Based Synthesis of Ag Nanocubes with High-Yield, *Sci. Rep.*, 2015, **5**, 10772.

43 J. L. Castro, S. Sanchez-Cortes, J. V. Garcia Ramos, J. C. Otero and J. I. Marcos, Surface-enhanced Raman spectroscopy of γ-aminobutyric acid on silver colloid surfaces, *Biospectroscopy*, 1997, **3**, 449–455.

44 J. S. Suh and M. Moskovits, Surface-Enhanced Raman Spectroscopy of Amino Acids and Nucleotide Bases Adsorbed on Silver, *J. Am. Chem. Soc.*, 1986, **108**, 4711–4718.
45 M. Stavytska-Barba and A. M. Kelley, Surface-Enhanced Raman Study of the Interaction of PEDOT:PSS with Plasmonically Active Nanoparticles, *J. Phys. Chem. C*, 2010, **114**, 6822–6830.
46 S. Garreau, G. Louarn, J. P. Buisson, G. Froyer and S. Lefrant, In situ spectroelectrochemical Raman studies of poly(3,4-ethylenedioxythiophene) (PEDT), *Macromolecules*, 1999, **32**, 6807–6812.
47 A. Lisowska-Oleksiak, A. P. Nowak, M. Wilamowska, M. Sikora, W. Szczerba and C. Kapusta, Ex situ XANES, XPS and Raman studies of poly(3,4-ethylenedioxythiophene) modified by iron hexacyanoferrate, *Synth. Met.*, 2010, **160**, 1234–1240.
48 B. R. Moraes, N. S. Campos and C. M. S. Izumi, Surface-enhanced Raman scattering of EDOT and PEDOT on silver and gold nanoparticles, *Vib. Spectrosc.*, 2018, **96**, 137–142.
49 S. Honary and F. Zahir, Effect of Zeta Potential on the Properties of Nano-Drug Delivery Systems – A Review (Part 2), *Trop. J. Pharm. Res.*, 2013, **12**, 265–273.
50 I. E. Stewart, M. Jun Kim and B. J. Wiley, Effect of morphology on the electrical resistivity of silver nanostructure films, *ACS Appl. Mater. Interfaces*, 2017, **9**, 1870–1879.
51 L. Cao, X. Bai, Z. Lin, P. Zhang, S. Deng, X. Du and W. Li, The Preparation of Ag Nanoparticle and Ink Used for Inkjet Printing of Paper Based Conductive Patterns, *Materials*, 2017, **10**, 1004.
52 L. Zhuo, W. Liu, Z. Zhao, E. Yin, C. Li, L. Zhou, Q. Zhang, Y. Feng and S. Lin, Cost-effective silver nano-ink for inkjet printing in application of flexible electronic devices, *Chem. Phys. Lett.*, 2020, **757**, 137904.
53 A. Kosmala, R. Wright, Q. Zhang and P. Kirby, Synthesis of silver nano particles and fabrication of aqueous Ag inks for inkjet printing, *Mater. Chem. Phys.*, 2011, **129**, 1075–1080.
54 W. Yang, F. Mathies, E. L. Unger, F. Hermerschmidt and E. J. W. List-Kratochvil, One-pot synthesis of a stable and cost-effective silver particle-free ink for inkjet-printed flexible electronics, *J. Mater. Chem. C*, 2020, **8**, 16443–16451.
55 I. J. Fernandes, A. F. Aroche, A. Schuck, P. Lamberty, C. R. Peter, W. Hasenkamp and T. L. A. C. Rocha, Silver nanoparticle conductive inks: synthesis, characterization, and fabrication of inkjet-printed flexible electrodes, *Sci. Rep.*, 2020, **10**, 1–11.
56 Z. Yu, Y. Xia, D. Du and J. Ouyang, PEDOT:PSS Films with Metallic Conductivity through a Treatment with Common Organic Solutions of Organic Salts and Their Application as a Transparent Electrode of Polymer Solar Cells, *ACS Appl. Mater. Interfaces*, 2016, **8**(18), 11629–11638.

